The Signal and Noise Analysis of Direct Conversion EHM Transceivers

Farnaz Shayegh*, Abbas Mohammadi*, Abdolali Abdipour*, Vafa Sedghi* and Rashid Mirzavand*

Abstract: A direct conversion modulator-demodulator with even harmonic mixers with emphasis on noise analysis is presented. The circuits consist of even harmonic mixers (EHMs) realized with antiparallel diode pairs (APDPs). We evaluate the different levels of I/Q imbalances and DC offsets and use signal space concepts to analyze the bit error rate (BER) of the proposed transceiver using M-ary QAM schemes. Moreover, the simultaneous analysis of the signal and noise has been presented.

Keywords: Even Harmonic Mixer (EHM), Direct Conversion Circuitry, Antiparallel Diode Pair (APDP), QAM Modulation, Signal and Noise.

1 Introduction

The cost reduction in wireless transceiver design is a key issue to increase the deployment of these systems. Among various realization techniques, the direct conversion implementation reduces the size and cost of the wireless transceivers. A direct conversion modulator-demodulator using even harmonic mixers (EHMs) is designed. The EHM is based on antiparallel diode pair (APDP). The APDP has a balanced structure that suppresses the fundamental mixing products. These products flow only within the APDP loop [1]. The EHM with APDP has some advantages that make it very attractive for millimeter-wave transceivers. These advantages are: (1) it can operate with halved LO frequency. (2) in direct conversion transmitter, it can suppress the virtual LO leakage(2) that locates nearby a desired RF signal. (3) it suppresses DC offset in direct conversion receivers.

The paper is organized as follows: The even harmonic mixer structure and three methods to improve its behavior are introduced. Then, a direct conversion modulator is designed using even harmonic mixers. The modulator structure is reciprocal and can also be used as a direct conversion demodulator. Next, we consider the effects of I/Q imbalances and DC offsets on the bit error rate performance of the demodulator. Finally, the simultaneous signal and noise analysis of the EHM structure has been presented.

Iranian Journal of Electrical & Electronic Engineering, 2006.
Paper first received 4th March 2006 and in revised form 1st March 2007.
* The Authors are with Microwave/MM-wave and Wireless Communication Research Lab., Electrical Engineering Department, AmirKabir University of Technology (Polytechnic), Tehran, Iran.
E-mail: abm125@aut.ac.ir , abdipour@aut.ac.ir.

2 Even Harmonic Mixer

Figure 1(a) shows a circuit configuration of the even harmonic mixer(EHM). It includes open and short circuited stubs at each port of the APDP. Both of them have a quarter-wave length at LO frequency. Using these stubs, the BPF and the LPF, the leakage of each port at other ports is suppressed [2].The BPF is designed to cover the RF band of 27.5-28.5 GHz. It is a third order chebycheve filter with center frequency of 28 GHz. The filter insertion loss (S12) and also the filter S11 curves in dB are shown in Fig. 2. As we can see from the filter insertion loss, the filter center frequency is 28 GHz and its 3-dB bandwidth is 1 GHz from 27.5 GHz to 28.5 GHz. In 28 GHz, the amount of S11 and S22 in dB is -28.674, so there is a good matching in filter input and output. The GaAs schottky barrier APDP (agilent HSCH-9551) is used to realize the mixer. Table 1 shows its parameters.

This mixer is used to mix the baseband signal (at 100 MHz) with the second harmonic of the LO signal (at 13.95 GHz) to provide the RF signal at 28 GHz. Figure 3 shows the mixer conversion gain versus LO power [3]. This results are obtained from the Harmonic-Balance simulation. Figure 1(b) shows the schottky diode nonlinear model. In continue, we introduce three ways to improve the mixer behavior and reduce its conversion loss.

2.1 Matching Networks

In this section matching networks in both sides of the APDP are included in an effort to reduce the mixer conversion loss and the LO power required for optimal mixer conversion loss [4]. LO matching network consists of a series delay line followed by a shunt short-circuited stub. RF matching network consists of a series delay line followed by a shunt open-circuited

stub. These matching networks are designed to match the APDP impedance at the LO and RF ports to 50 ohm. The length of these stubs are iteratively tuned to provide good conversion loss at a relatively low LO drive level. Figure 4 shows the mixer conversion gain versus LO power with and without the matching networks. As we can see from this figure, matching networks result in decrease of LO power required for optimal mixer conversion loss and a slight improvement in mixer conversion loss.

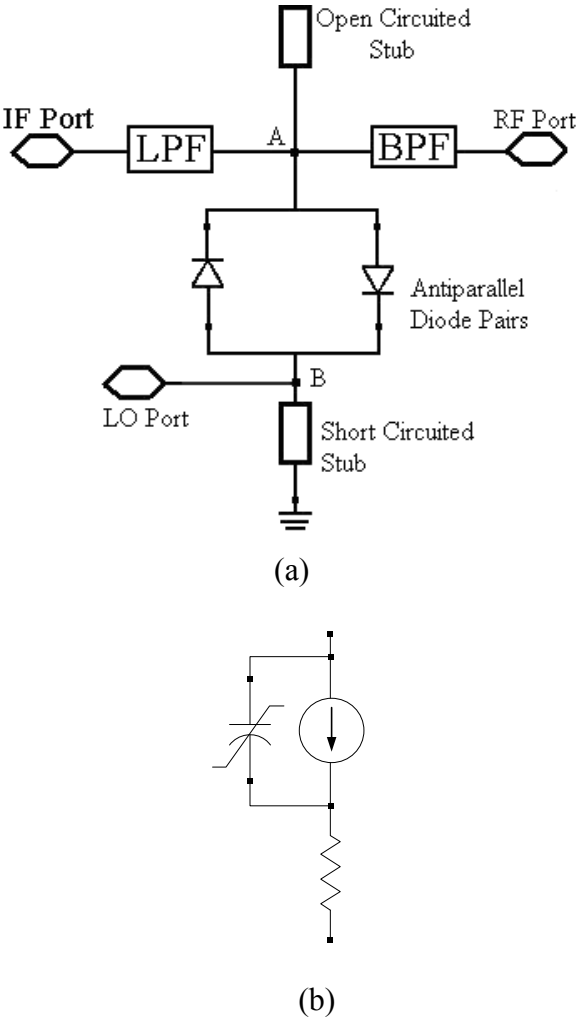

Fig. 1 a) Circuit configuration of the even harmonic mixer, b) Schottky diode nonlinear model.

Table 1 Diode parameters.

Junction Capacitance (Cj0)	0.04 pF
Series Resistance (Rs)	6 Ω
Saturation Current (Is)	1.6E-13 A
Ideality Factor (N)	1.2

2.2 Parallel diodes

As we know, series resistance (Rs) of schottky diodes is a major factor in diode mixer conversion loss. If two parallel schottky diodes are substituted for each diode in APDP, effective Rs of the structure will be divided by an approximate factor of two and the conversion loss will be decreased [5]. Also use of three diodes instead of each diode causes more decrease in mixer conversion loss. For each of above cases, matching networks should be designed again. Figure 5 shows the mixer conversion loss with one, two and three diodes.

2.3 Self-biased APDP

Another way to improve the conversion loss of our mixer is to use self-biased APDP [6]. In this case RC networks in both sides of each diode are designed to flatten the conversion loss of the even harmonic mixer. The values of RC networks are: R=150 ohm, C=50 pf. Figure 6 shows conversion gain versus LO power with self-biased APDP and conventional APDP. The conversion loss of EHM using self-biased APDP is almost constant from 10 dBm to 25 dBm of LO power.

2.3.1 Numerical Results

We also write a program with Matlab software in order to calculate the conversion loss of the EHM using self-biased APDP by the Harmonic Balance method. Diode parameters used for calculation are obtained from the agilent HSCH-9551 data sheet. We set the RF frequency to 28 GHz and the RF power to -75 dBm. The RF signal is mixed with second harmonic of the LO signal. Figure 7 shows calculated conversion gain versus LO power. As may be seen, the calculated results agree well with the simulated results. In order to have the best mixer behavior, self-biased APDP is used and three diodes are substituted for each diode in APDP. In addition to this matching networks are designed in both sides of the APDP. Figure 8 shows the mixer structure used in our design. In continue, we consider the third order intermodulation results [7]. To do this, two sinusoidal signals at the same amplitude and little frequency difference (28.007 GHz, 27.93 GHz) are inserted at the RF port and input and output IP3 (3th order Intercept Point) are calculated. Figure 9 shows the results.

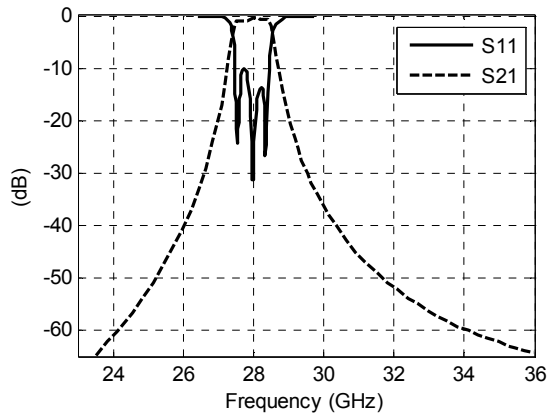

Fig. 2 Filter S11 and S12 (in dB).

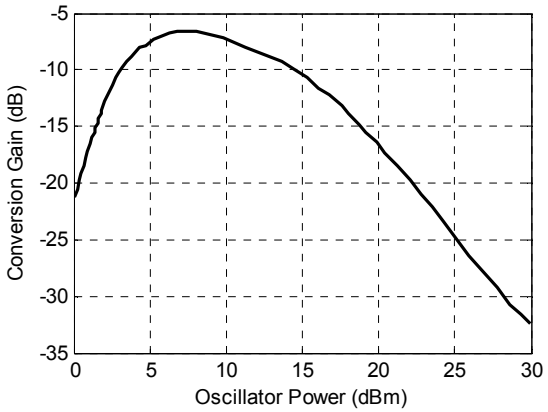

Fig. 3 Conversion gain of the EHM.

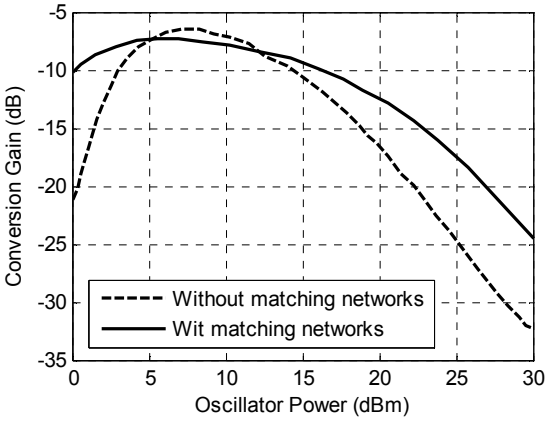

Fig. 4 mixer conversion gain using one diode, solid line: with matching networks, dashed line: without matching networks.

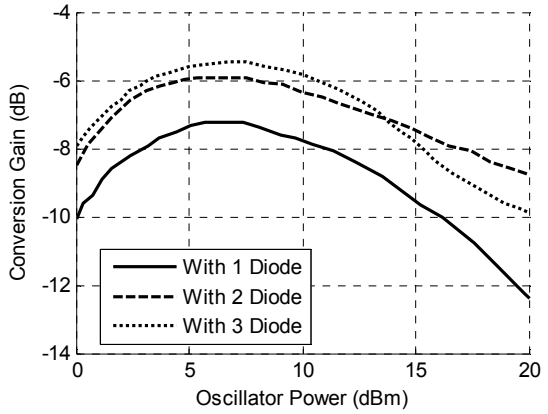

Fig. 5 mixer conversion gain.

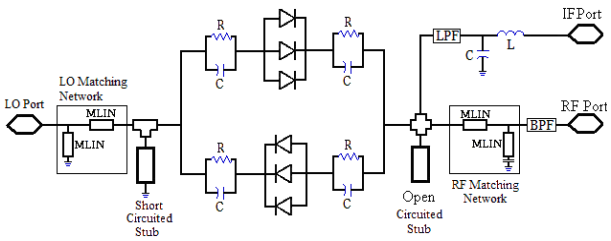

Fig. 8 EHM structure used in our design.

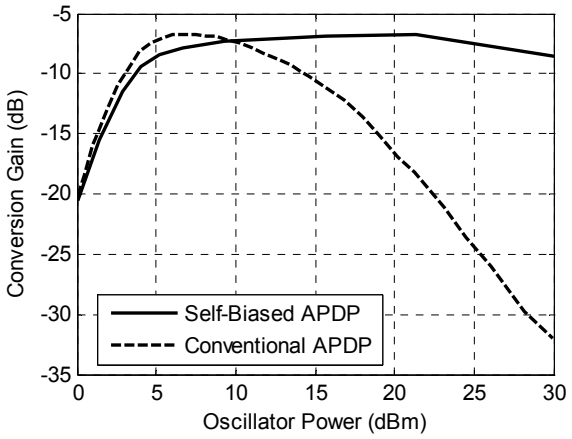

Fig. 6 Conversion gain of the EHM using self-biased APDP and conventional APDP.

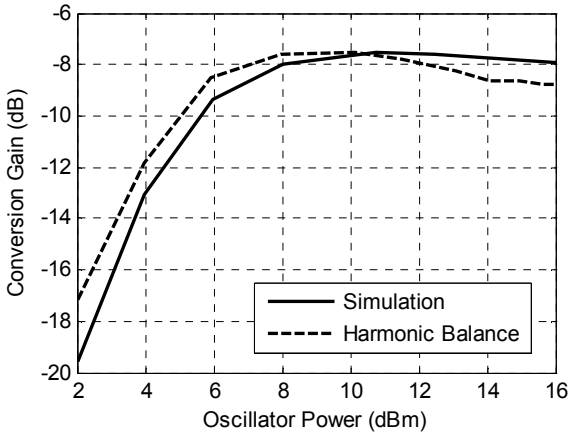

Fig. 7 Conversion gain of the EHM using self-biased APDP calculated by the Harmonic Balance method and compared with simulated results.

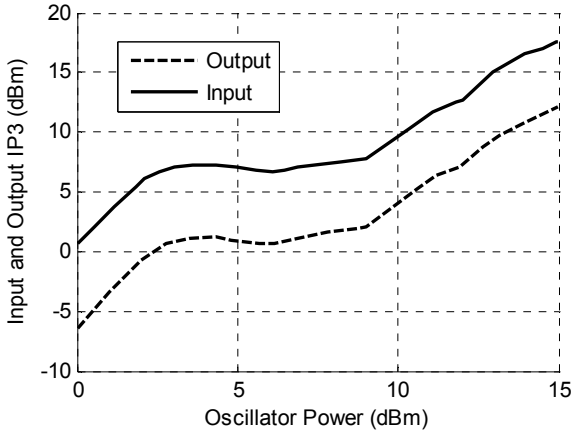

Fig. 9 Input and output IP3 versus LO power for self-biased EHM.

3 Modulator Structure

The proposed I-Q modulator consists of two even harmonic mixers. The LO signal is splited by a Wilkinson power divider, and a delay line is connected to one of Wilkinson power divider arms to provide phase difference at the second harmonic of the LO [8]. The LO carriers are mixed with baseband modulating signals (I & Q) in even harmonic mixers. Finally, both mixed signals are combined in a Wilkinson power combiner and the modulated signal is produced.
The following formulas illustrate the modulator inputs:

$$v_{LO}(t)=\cos\omega_{LO}t \quad (1)$$

$$v_{I}(t)=\cos\omega_{IF}t \quad (2)$$

$$v_{Q}(t)=\cos(\omega_{IF}t+90) \quad (3)$$

Then, the outputs of EHMs can be obtained as follows:

$$e_1(t)=\cos2\omega_{LO}t\times\cos\omega_{IF}t \quad (4)$$

$$e_2(t)=\cos(2\omega_{LO}t-90)\times\cos(\omega_{IF}t+90) \quad (5)$$

Finally, using Wilkinson power combiner, the modulated signal is as:

$$e(t)=e_1(t)+e_2(t)=\cos(2\omega_{LO}+\omega_{IF})t \quad (6)$$

As may be seen, the lower sideband component ($2f_{LO}$-f_{IF}) is suppressed without external filters.
In order to characterize the modulator performance, we insert two sinusoidal carriers at the same low frequency (f_{IF}=100MHz), same amplitude and quadrature phase on the I and Q inputs. Figure 11 shows the RF spectrum of the modulator operating at LO power of 10 dBm and LO frequency of 13.95 GHz. The power of virtual LO leakage ($2f_{LO}$ =27.9 GHz) is -67 dBm. So, the suppression of the virtual LO leakage of 77 dB is obtained. The lower sideband component ($2f_{LO}$-f_{IF}=27.8 GHz) is 25 dB lower than the desired component ($f_{RF}=2f_{LO}+f_{IF}$=28 GHz).
Figure 12 shows the conversion gain of the whole modulator using a self-biased APDP and a conventional APDP.

4 Demodulator

As mentioned above, the modulator is realized with passive components and the mixer is based on schottky diodes that don't need DC bias circuitry. Accordingly, the whole modulator has zero DC power consumption. This modulator is totally reciprocal and can be used as a demodulator [9]. To characterize this circuit as a demodulator, a sinusoidal signal is inserted on RF port and the power at I & Q outputs is measured. Figure 12 shows conversion gain of the demodulator versus RF frequency from 26 to 30 GHz. The figure shows that the demodulator has bandwidth better than 1.5 GHz. The average conversion loss is 7.5 dB around 28 GHz for both channels.

5 BER Calculations

In this section we consider the impacts of I/Q imbalances and DC offsets on QAM detection in the demodulator. The input signal in the RF port is a QAM signal and can be written as follows:

$$X_{RF}(t)=\sqrt{\frac{2E_{min}}{T_s}}(a_i\cos(2\pi f_c t)+b_i\sin(2\pi f_c t)) \quad (7)$$

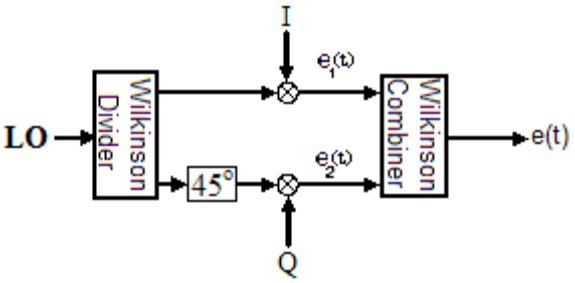

Fig. 10 Modulator structure.

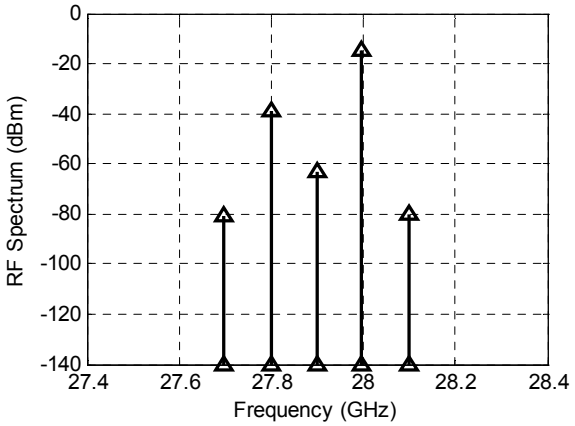

Fig. 11 Spectrum at output of the modulator.

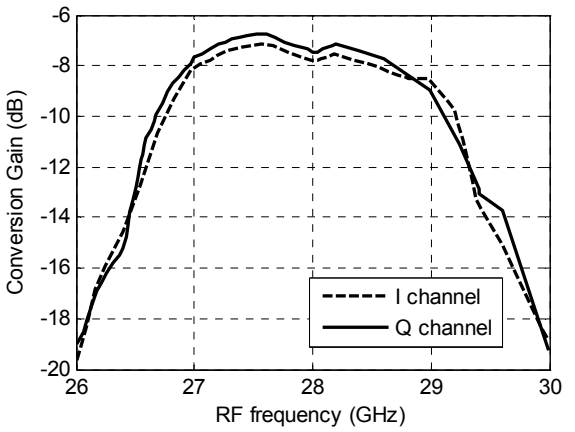

Fig. 12 Conversion gain versus RF frequency for I & Q channels at LO power of 10 dBm.

where:

$$\{a_i,b_i\}=\begin{bmatrix}(-L+1,L-1)(-L+3,L-1)...(L-1,L-1)\\(-L+1,L-3)(-L+3,L-3)...(L-1,L-3)\\.....\\.....\\(-L+1,-L+1)(-L+3,-L+1)...(L-1,-L+1)\end{bmatrix} \quad (8)$$

and $i=1,2,L,L$; $L=\sqrt{m}$.

M is restricted to 2^P so that each symbol can be represented by P bits. We will restrict our consideration to Gray code bit mapping [10]. The Gray code mapping has the property that two P-bit symbols corresponding to adjacent symbols differ in only a single bit. As a result, an error in an adjacent symbol is accompanied by one and only one bit error. Finally, we do our calculations under AWGN channel.

5.1 BER Calculations in Presence of I/Q Imbalances

We assume that the I and Q paths of LO signal in the demodulator are equal to:

$$X_{Lo,I}(t)=(1+\varepsilon/2)\cos(\omega_{Lo}t+\theta/2) \quad (9)$$

$$X_{Lo,Q}(t)=(1-\varepsilon/2)\cos(\omega_{Lo}t-\theta/2) \quad (10)$$

where ε and θ represent gain and phase errors, respectively. As we know from [1], the conductance expression for an APDP can be written as:

$$g=2\alpha i_s\cosh(\alpha V) \quad (11)$$

In this formula, α and i_s are the slope ($\alpha=q/kT$) and saturation current of diodes. For the usual case in which only the LO signal modulates the conductance of the diodes we may substitute $V=X_{Lo}(t)$. So conductances in I and Q paths may be expanded in the following series [1]:

$$g_I=2\alpha i_s[I_0(\alpha(1+\varepsilon/2))+2I_2(\alpha(1+\varepsilon/2))\cos(2\omega_{Lo}t+\theta)+...] \quad (12)$$

$$g_Q=2\alpha i_s[I_0(\alpha(1-\varepsilon/2))+2I_2(\alpha(1-\varepsilon/2))\sin(2\omega_{Lo}t-\theta)+...] \quad (13)$$

Where I_n are modified Bessel functions of the first kind. So, the output currents in I and Q ports after a lowpass filter are equal to:

$$\tilde{I}=2\alpha i_s\sqrt{\frac{2E_{min}}{T_s}}I_2(\alpha(1+\varepsilon/2))[a_i\cos\theta-b_i\sin\theta] \quad (14)$$

$$\tilde{Q}=2\alpha i_s\sqrt{\frac{2E_{min}}{T_s}}I_2(\alpha(1-\varepsilon/2))[b_i\cos\theta-a_i\sin\theta] \quad (15)$$

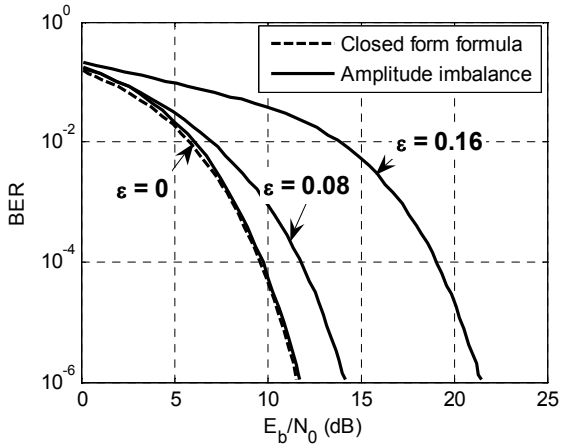

Fig. 13 BER of the 16 QAM signal versus Eb/N0 as a function of ε. From left to right ε=0, 0.08, 0.16. Dashed line represent BER calculated from the closed form formula.

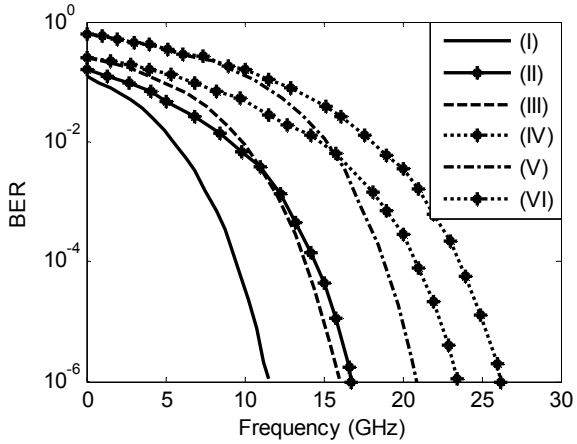

Fig. 14 BER versus Eb/N0 for 16, 64, 256-QAM in permitted ranges of amplitude error. From left to right:
(I)16-QAM: ε=0, (II) 16-QAM: ε = 0.12,
(III) 64-QAM: ε=0, (IV) 64-QAM: ε=0.03,
(V) 256-QAM: ε=0, (VI) 256-QAM: ε=0.014.

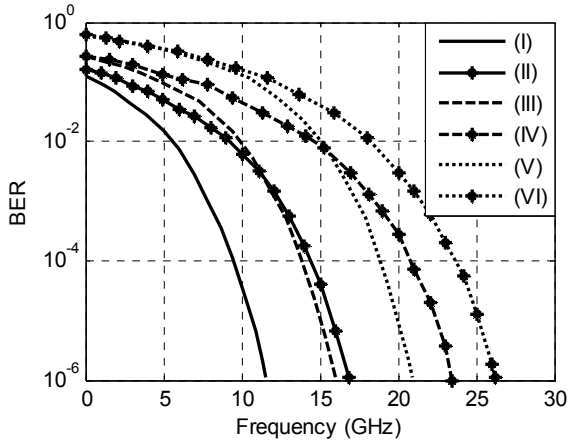

Fig. 15 BER versus Eb/N0 for 16, 64, 256-QAM in permitted ranges of phase error. From left to right:
(I)16-QAM: θ =0, (II) 16-QAM: θ =9,
(III) 64-QAM: θ =0, (IV) 64-QAM: θ =5,
(V) 256-QAM: θ =0, (VI) 256-QAM: θ =2.

It can be seen that in either case, the errors in the nominally 45° phase shifts and mismatches between the amplitudes of the I and Q signal corrupt the downconverted signal constellation, thereby rising the bit error rate. In continue, we calculate the BER for different levels of amplitude and phase imbalances. For this purpose we use the signal space concepts described in [11]. We derive algorithms to do these calculations for 16, 64 and 256-QAM schemes. We also use approximate closed form formula in equation (16) to compare our results with:

$$BER=\frac{4}{\log_2 M}(1-\frac{1}{\sqrt{M}})Q(\sqrt{\frac{3(Eb/N0)\log_2 M}{(M-1)}}) \qquad (16)$$

Firstly we assume amplitude imbalance. Figure 13 shows the BER of the 16-QAM signal for ε values of 0, 0.08, 0.16. It also illustrates the BER obtained from closed form formula that is in agreement with our result for ε=0. From the figure, it can be seen that as the amplitude error increases, the amount of Eb/N0 required having BER of 10e-6 increases. In 16-QAM modulation, if the amplitude error in I and Q paths reaches 28 percent, the BER will be irreducible. This error for 64 and 265-QAM is 11 and 5 percent respectively. Figure 14 illustrates BER of 16, 64 and 256-QAM schemes in permitted ranges of amplitude error. In continue we consider phase errors. Like amplitude error as phase error increases the amount of Eb/N0 required to have BER of 10e-6 increases. In 16-QAM modulation, if phase error in I and Q paths reaches 20 degree, the BER will be irreducible. This error for 64 and 256-QAM is 9 and 4 degree respectively. Figure 15 shows BER of 16, 64 and 256-QAM schemes in permitted ranges of phase error. So in M-ary QAM, as M increases, the amount of permitted amplitude and phase errors reduces and the amount of BER increases.

5.2 BER Calculations in Presence of DC Offsets

The unbalance effects in APDP created by mismatch in the IV characteristics of diodes causes DC offsets. If saturation currents i_s and slope parameters α are different for the two diodes of the APDP, we may assume that:

$$i_{s1}=i_s+\Delta i_s \quad , \quad i_{s2}=i_s-\Delta i_s \qquad (17)$$

$$\alpha_1=\alpha+\Delta\alpha \quad , \quad \alpha_2=\alpha-\Delta\alpha \qquad (18)$$

As we know from [4], the conductance expressions for i_s and α mismatches can respectively written as

$$g_{\Delta i_s}=2\alpha i_s[\cosh\alpha V+\frac{\Delta i_s}{i_s}\sinh\alpha V] \qquad (19)$$

$$g_{\Delta\alpha}=2\alpha i_s e^{(\Delta\alpha)V}[\cosh\alpha V+\frac{\Delta\alpha}{\alpha}\sinh\alpha V] \qquad (20)$$

Like previous section, we multiply these conductances to the applied voltage. The output current of the APDP has a DC offset that is equal to:

$$i_{dc\text{-}offset}=2\alpha i_s V_{Lo} I_1(\Delta\alpha V_{Lo})\times[I_0(\alpha V_{Lo})+I_2(\alpha V_{Lo})] \pm 2\alpha(\Delta i_s)V_{Lo}I_1(\alpha V_{Lo}) \qquad (21)$$

Current terms add constructively when one of the diodes has both a higher slope and higher saturation current. They add destructively otherwise. So the output currents in I and Q paths after a lowpass filter are equal to:

$$\tilde{I}=2\alpha i_s\sqrt{\frac{2E_{min}}{T_s}}I_2(\alpha V_{Lo})a_i+i_{dc\text{-}offset} \qquad (22)$$

$$\tilde{Q}=2\alpha i_s\sqrt{\frac{2E_{min}}{T_s}}I_2(\alpha V_{Lo})b_i+i_{dc\text{-}offset} \qquad (23)$$

$\Delta\alpha$ and Δi_s may be different in I and Q paths. So, the signal constellation is corrupted and the BER increases. In continue, we calculate the BER due to different levels of diode imbalances. As the mismatches increase, the amount of Eb/N0 required to have BER of 10e-6 increases. For example in 16-QAM signal, we consider different cases of mismatch that are shown in Fig. 16. It can be seen that the effect of α mismatch on BER degradation is more than i_s mismatch [12].

6 Simultaneous Signal and Noise Analysis of the EHM Structure

The signal and noise analysis of the EHM structure of the Fig. 1 is presented in this section. The method can be decomposed into two main algorithms: The nonlinear steady state solution and linear perturbation analysis. Under the large signal excitation of a local oscillator there exist stable, time-periodic solutions for the mixer. In the next step the effect of superimposing the signal and noise on such periodic steady state waveform is analyzed assuming that the signal and noise spectral components are small compared to local oscillator.

The circuit is shown in Fig. 17. The nonlinear simulation engine is HB, which is quite mature and generally considered accurate and appropriate for circuits with any degree of nonlinearity. The detail of this technique can be found at [13].Generally this method is based on the principle that, for a sinusoidal excitation, the steady state solution of the network node voltages and currents, can be approximated using Fourier series. The circuit is divided into linear and nonlinear subcircuit multiport network, with each element in the nonlinear subcircuit connected to ports in the linear sub circuit.

The input signal source is omitted and the corresponding port is loaded with generator

impedance. The load of IF port is the input impedance of an IF amplifier. The accuracy of the steady state nonlinear behavior improves as more harmonics of the fundamental excitation are included. Ignoring harmonics above the M^{th} is equivalent to assuming finite real embedding impedances Z_0 at the higher harmonics. In our EHM structure the diode capacitance form a low impedance shunt across the embedding network.

Figure 18 shows a complete view of the circuit including all noise sources. The a and e consequently indicate linear to nonlinear and linear to external source and load interconnections. Pumping the diodes result in a periodic conductance a capacitance.

That can be presented in form of Fourier series, contain harmonics of local oscillator. Knowing these Fourier series coefficients, it is possible top to construct the small signal conversion matrix for the diode pair [14].

$$\delta I = Y \delta V \tag{24}$$

Assuming RF signal is small enough both δI and δV contain components at only the pair of side-frequencies $k\omega_{Lo} \pm \omega_{RF}$.

The admittance matrix Y allows the pumped diode to be treated as a multi-frequency multi-port network with one port for each sideband frequency. Combing this multi-frequency linear representation of nonlinear elements with the linear section, results in an equivalent Y matrix, Y_{eq}, that may any circuit specification can be extracted of this matrix by properly chosen ports. Figure 19 indicates the multi-port circuit concept. In this figure R_s is included in the linear network. So the related thermal noise source is absorbed by J_{La1} and J_{La2}.

To perform the noise analysis, noise correlation of each group of noise sources should be calculated. First noise source group is related to linear network. The correlation matrix is calculated directly from signal parameters of the network.

$$C_j = 2kT\Delta f([Y]+[Y]^{*t}) \tag{25}$$

Second correlation matrix is related to the sources of the signal, represented by C.

$$C = \begin{cases} \langle J_{ei} J_{ej}^{*t} \rangle & i^t j \\ 0 & \text{otherwise} \end{cases} \tag{26}$$

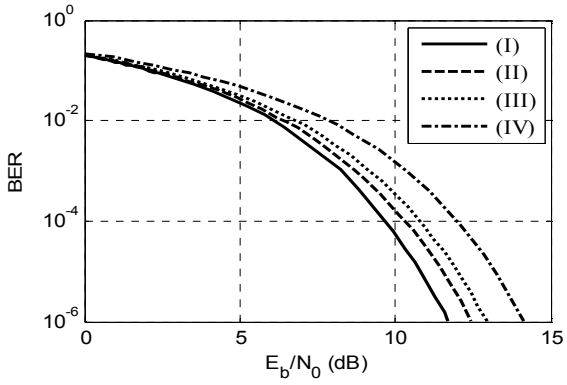

Fig. 16 BER of 16-QAM signal for different levels of diodes mismatches. From left to right: (I) without mismatch, (II) i_s mismatch of 10%, (III) α mismatch of 10% and (IV) both α and i_s mismatch of 10%.

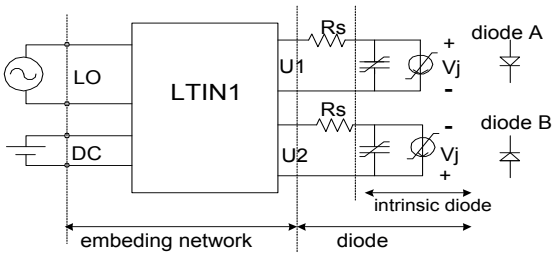

Fig. 17 The circuit presentation for the steady state response in simultaneous signal and noise analysis based on HB nonlinear analysis. In proposed SHP mixer no DC bias is needed.

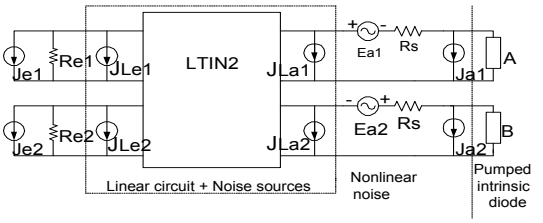

Fig. 18 The circuit presentation for the small signal and noise analysis.

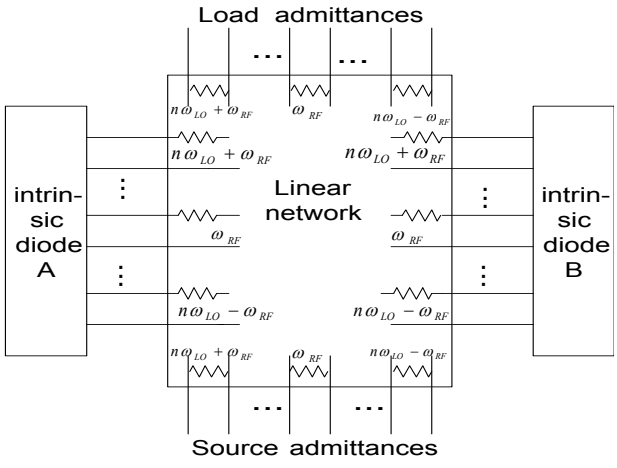

Fig. 19 The multi-frequency, multi-port presentation of the circuit.

The last noise sources are related to nonlinear elements of the circuit. The shot noise in each diode can likewise be regarded as amplitude modulated Gaussian noise. Due to independent physical process of shot noise generation in two diodes, there is no correlation between the unmodulated noises. The modulation process generates additional sideband at each diode. Since their unmodulated components are not correlated, there will be no correlation between the modulated noise components. Thus C_{ja} is diagonal.

$$C_{ja}=\acute{a}\begin{pmatrix}J_{a1}\\J_{a2}\end{pmatrix}\left(J_{a1}^{*}J_{a2}^{*}\right)\tilde{n} \qquad (27)$$

Proper combination of this correlation matrices result in a global correlation matrix. By this matrix, noise power of output port at desired frequencies.
For calculating the noise figure, $\left|\bar{V}(\omega_{IF})\right|^2$ component of the matrix is used.

6.1 Pure Resistive Model

First step in diode nonlinear modeling is to model it as a pure resistive model with no capacitance. In the used diodes I_s=1.6e-13, R_s=5Ω. The current of the diode pair is the summation of each diode's current.
Therimionic emission theory can be used to characterize the Schottky-barrier diode. When the ratio of ratio of minority carrier is small, the diodes' current are:

$$i_1=i_s\{\text{Exp}(\alpha(v-i_1R_s))-1\} \qquad (28\text{-a})$$

$$i_2=-i_s\{\text{Exp}(\alpha(-v+i_2R_s))-1\} \qquad (28\text{-b})$$

v is the applied voltage to the diode, R_s is series resistance and α is the abbreviation of q/nkT. No DC bias is applied to these diodes. When simplifying assumption is used [2] the APDP current become

$$i=i_1+i_2=2\alpha i_s\text{Sinh}(\alpha(v-iR_s)) \qquad (29)$$

the conductance of the diode pair is

$$g=\frac{di}{dv}=\frac{2\alpha i_s\text{Cosh}(\alpha v)+4\alpha^2 i_s^2R_s}{1+2\alpha i_sR_s\text{Cosh}(\alpha v)} \qquad (30)$$

To determine the APDP steady state performance, g should be further simplified. When R_s is zero, or equivalently the applied voltage is to the junction voltage, g can be expanded in a Fourier series form:

$$g=y_0+2y_1\text{Cos}2\omega_pt+\cdots$$

$$y_n=2\alpha i_sI_n(\alpha v_p) \qquad (31)$$

The noise figure of the structure has been presented in Figure 20 in the different oscillator power.

6.2 Constant Junction Capacitance Model

In this part just capacitive effect of the diode is modeled just by a constant one. By developing the software to this purpose the results are as fallow. Including just even harmonics in conductance or just odd harmonics in the current, is attractive for EHM structure. The simplest form of these mixers contains an APDP as a mixing core and two stubs as filters. A short one-quarter wavelength long stub at LO frequency grounds the 2LO, or approximately the RF signal. The open stub at the other side, pass the RF signal and suppress LO because of being short at that frequencies. The BPF at the RF port and band reject filter at IF port, reject undesired mixing components and preventing port leakage to RF port.

6.3 Dynamic Junction Capacitance Model

The full model of the diode in this stage has been used. The conversion loss and the noise figure of the structure in different oscillator has been presented in Fig. 21.

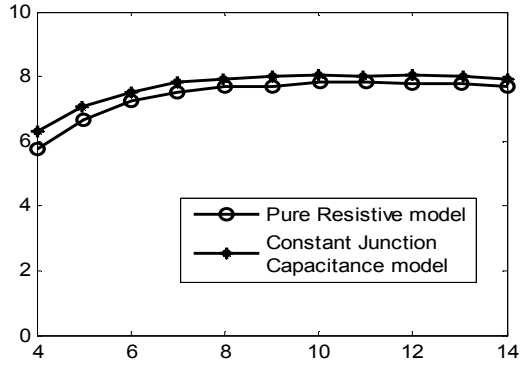

Fig. 20 The comparison of noise figure in resistive and constant capacitance model (NF and PLO are in dB and dBm, respectively).

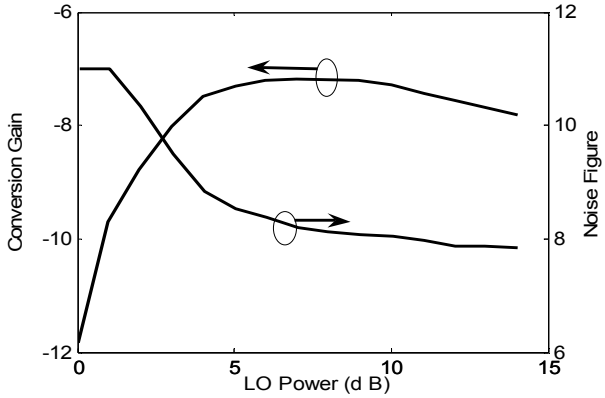

Fig. 21 The conversion gain and noise figure of the dynamic model (Gain and LO power are in dB)

7 Conclusion

Direct conversion circuitry with even harmonic mixers based on Antiparallel Diode Pair (APDP) was used to realize a Ka-Band even harmonic quadrature modulator-demodulator operating at 28GHz. Self-biased APDP was used in order to flatten the conversion loss of the system versus LO power. The system structure is very attractive, because of reducing hardware complexity and cost. The impacts of I/Q imbalances and DC offsets on BER performance of the system was also considered. Moreover, the simultaneous analysis of the signal and noise has been presented.

Acknowledgement

The authors wish to thank the editor and the anonymous reviewers for their insightful comments and suggestions which greatly improved the presentation of this work. This work was supported in part by Iran Telecommunication Research Center (ITRC) and academic research section of Iran Management and Planning Organization (#102) under contract 1721.

References

[1] M. Cohn, J. E. Degenford and B. A. Newman, "Harmonic mixing with an antiparallel diode pair,", *Proc. IEEE Trans. on Microwave Theory Tech*., vol.MTT-23,8, pp.667-673, Aug. 1975.

[2] K. Itoh, A. Ida, Y. Sasaki, and S. Urasaki, "A 40GHz band monolithic even harmonic mixer with an antiparallel diode pair," *Proc. IEEE MTT-S Int. Microwave Symp*. Digest, pp.879-882, June 1991.

[3] M. R. Barber, "Noise figure and conversion loss of the schottky barrier diode," *Proc. IEEE Trans. Microwave Theory & Tech*., vol. MTT-15, No.11, pp. 629-635, Nov. 1967.

[4] C.J. Verner, D. Drolet, M.G. Stubbs and C. Pike, "Development of a ka-Band Even Harmonic Modulator for a Satellite Briefcase Terminal," *Proc. IEEE*, pp. 448-451, 1999.

[5] M. W. Chapman, and S. Raman, "A 60 GHz Uniplanar MMIC Subharmonic Mixer," *Proc. IEEE MTT-S Digest*, pp. 95-98, 2001.

[6] M. Shimozawa, T. Katsura, K. Maeda, E. Taniuchi, T. Ikushima, N. Suematsu, K. Itoh, "An Even Harmonic Mixer using Self-Biased Anti-Parallel Diode Pair", *Proc. IEEE MTT-S Int. Microwave Symp. Dig*, pp. 253-256, vol. 1, June 2002.

[7] P. Blount, C. Trantanella, "A High IP3, Subharmonically Pumped Mixer for LMDS Applications", *Proc. IEEE GaAs Digest*, pp. 171-174, 2000.

[8] J. Y. Park, S. Jeon, Y. Wang, T. Itoh., "Integrated Antenna with Direct Conversion Circuity for Broad-Band Millimeter-Wave Communications", *Proc. IEEE Trans. Microwave Theory Tech*, vol. 51, No. 5, MAY 2003.

[9] I. Telliez, A. Couturier, C. Rumelhard, C. Versnaeyen, "A compact monolithic microwave demodulator-modulator for 64-QAM digital radio link", *Proc. IEEE Trans. Microwave Theory Tech*., MTT-39, no. 12, pp. 1947-1954, Dec. 1991.

[10] P. J. Lee, "Computation of the bit error rate of coherent M-ary PSK with Gray code bit mapping," *Proc. IEEE Trans*., vol. COM-34, pp. 488-491, May 1986.

[11] Lu. Jianhua, K. B. Letaief, Justin C-I Chuang, Ming L. Liou, "M-PSK and M-QAM BER Computation Using Signal-Space Concepts," *Proc. IEEE Trans*. vol. 47, No. 2, 1999.

[12] F. Shayegh, A. Mohammadi, A. Abdipour, "Characterization of EHM Direct Conversion Transceivers in Ka Band", Proc. *EUMC 2005*, Paris, Oct. 2005.

[13] S. A. Mass, *Microwave Mixers,* Artech House, 1986.

[14] A. R. Kerr, "Noise and loss in balance and sub harmonically pumped mixers: part I-Theory," and "part 2-Experiments," *IEEE Trans. Microwave TheoryTech*, vol. MTT-27, pp. 938-950, Dec. 1979.

Farnaz Shayegh received B.Sc. in Electrical Engineering from Isfahan University of Technology and M.Sc. degree from AmirKabir University of Technology in 2006 in Electrical Engineering.

Abbas Mohammadi was born in Tehran, Iran. He received the B.Sc. degree in Electrical Engineering from Tehran University, Iran in 1988, the M.Sc. and Ph.D. degrees in Electrical Engineering from the University of Saskatchewan, Canada, in 1995, and 1999, respectively. He was a researcher at Telecommunications Research Lab (TRLabs), Canada, from 1995 to 1998. In December 1998, he joined to Wavecom Electronics, Microwave Research Lab, Victoria, Canada, as a senior research engineer where he conducted research on Microwave and Wireless Communications. Since March 2000, he has been with the Electrical Engineering Department of Amirkabir University of Technology (Tehran Polytechnic), Tehran, Iran, where he is currently the director of Communications Group. He has published over 70 Journal and Conference papers and holds three U.S. and one Canadian Patents. His current research interests include broadband wireless communications, adaptive modulation, MIMO Systems, Mesh and AdHoc Networks, Microwave and Wireless Subsystems, and direct conversion transceivers.

Abdolali Abdipour (M'97–SM'06) was born in Alashtar, Iran, in 1966. He received the B.Sc. degree in electrical engineering from Tehran University, Tehran, Iran, in 1989, the M.Sc. degree in electronics from Limoges University, Limoges, France, in 1992, and the Ph.D. degree in electronic

engineering from Paris XI university, Paris, France, in 1996. He is currently a Professor with the Electrical Engineering Department, AmirKabir University of Technology (Tehran Polytechnic), Tehran, Iran. He authored two books, *Noise in Electronic Communication: Modeling, Analysis and Measurement* (AmirKabir Univ. Press, 2005, in Persian) and *Transmission Lines* (Nahre Danesh Press, 2006, in Persian). His research areas include wireless communication systems (RF technology and transceivers), RF/microwave/millimeter-wave circuit and system design, electromagnetic (EM) modeling of active devices and circuits, high-frequency electronics (signal and noise), nonlinear modeling, and analysis of microwave devices and circuits. He has authored or coauthored over 115 papers in refereed journals and local and international conferences. Currently he is Head of Electrical Engineering Department, AmirKabir University of Technology (Tehran Polytechnic) and also Director of Radiocommunication Center of Excellence.

Vafa Sedghi received B.Sc. in Electrical Engineering from Sharif University of Technology and M.Sc. degree from AmirKabir University of Technology in 2006 in Electrical Engineering.

Rashid Mirzavand was born in Boroojen, Iran in 1983. He received B.Sc. in Electrical Engineering in 2004 from Isfahan University of Technology and M.Sc. degree from AmirKabir University of Technology in 2007 in Electrical Engineering. He is working toward Ph.D. degree in Electrical Engineering at the same university, since 2007. His research interests are in the areas of wireless communication systems, microwave instrumentation (six-port techniques) and computational electromagnetic.